A 2-D LINEAR ELASTIC MODEL FOR THE LOCAL OXIDATION OF SILICON USING THE BOUNDARY ELEMENT METHOD

M. J. Needs, V. Jović, C. Taylor, K. Board, M. J. Cooke

Faculty of Applied Science, University College of Swansea
Singleton Park, SWANSEA SA2 8PP, U.K.

ABSTRACT

Proceeding from a natural extension of the one-dimensional Deal and Grove relationship [2], a Boundary Element based numerical model has been developed which is used to simulate the local oxidation of silicon in two dimensions. A simple, two-step approach has been adopted, to predict the kinetics of oxide growth in wet or dry ambients and at certain process temperatures. This involves steady-state linear diffusion of the oxidising species in the silicon dioxide, followed by a linear elastic analysis of the boundary motion. By devoting particular attention to the control of error-inducing mechanisms inherent in the discretisation of the space and time domains, a reliable and efficient computer code has been developed which provides excellent representation of this complex, moving boundary problem.

1. INTRODUCTION

There is an on-going demand upon the semi-conductor industry to continually increase the complexity and versatility of the integrated circuits produced. This necessarily involves a reduction in the dimensions of electronic devices, whilst maintaining their reliability of performance and improving the cost-effectiveness of the fabrication procedure. It is readily observed that the packing density of integrated circuits is limited by the intrusion of the field oxide beneath the nitride masking film, and so the understanding and control of the oxidation process is crucial to the advancement of technology in this field.

In most commercial enterprises, the oxidation of silicon is a thermal process, during which the oxidising species diffuse through the oxide and then react with the high-purity silicon at the silicon/oxide interface. The oxidising species is O_2

when oxidation is by dry oxygen, and H_2O when oxidation is by wet oxygen. The chemical reaction at the silicon/oxide interface is attended by a growth of the oxide which consumes the silicon substrate. Because of the density difference between silicon and silicon dioxide, there is an overall increase in volume, which results in the movement of the free surface of the oxide into the gas phase.

Analytical techniques and long-established one-dimensional models (cf [2]), describing the kinetics of silicon oxidation, have proved inadequate when confronted with truly two-dimensional domains and the development of more sophisticated numerical models, together with the associated production of reliable and robust computer code, are vital pre-requisites to the advancement of semi-conductor microtechnology.

The current research programme seeks to model the 'bird's beak' phenomenon, and this paper describes the development of boundary element based software, providing a computer based numerical model of the oxidation of silicon, at process temperatures within the range of elastic behaviour for the materials under consideration.

2. PROBLEM DEFINITION

The model proposed here for the two-dimensional oxidation of silicon concerns linear diffusion of the oxidising species, together with linear elastic displacement of the dioxide and nitride layers, involving the solution of two uncoupled boundary value problems at each timestep.

2.1 Diffusion of the Oxidising Species

The initial part of the physical process is the diffusion of the oxidising species within the silicon dioxide. A limiting assumption is that the effective diffusivity of the oxidant is spatially invariant and dependent only on the process temperature and partial pressure of the oxidant. For the purposes of this analysis it has also been assumed that all transient terms can be neglected, so we therefore consider a problem of linear, steady-state diffusion, as detailed below.

Consider a sample of silicon covered by a thin pad oxide in the presence of a nitride mask.

Figure 1 depicts the dioxide (Ω_1) and nitride (Ω_2) domains at some intermediate state of the oxidation process.

The problem may be defined thus:

$$\text{Solve } \frac{\partial}{\partial x_i}\left(D_e \frac{\partial c}{\partial x_i}\right) = 0 \text{ inside } \Omega_1 \qquad i = 1,2 \qquad (1)$$

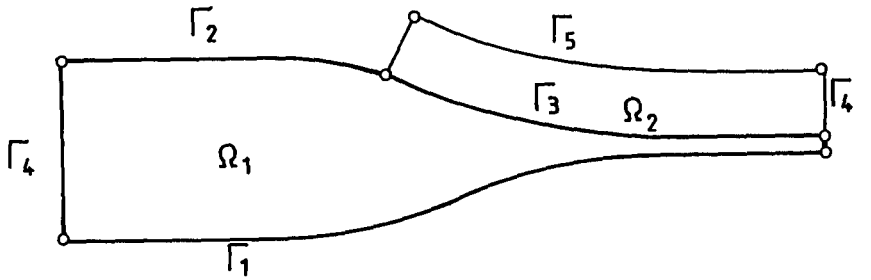

FIGURE 1

Subject to the following boundary conditions:

$$D_e \frac{\partial c}{\partial n} = k.c \qquad \text{on } \Gamma_1 \qquad (2)$$

$$D_e \frac{\partial c}{\partial n} = h(c-c^E) \qquad \text{on } \Gamma_2 \qquad (3)$$

$$D_e \frac{\partial c}{\partial n} = 0 \qquad \text{on } \Gamma_3 \cup \Gamma_4 \qquad (4)$$

where,

c = concentration of the oxidising species in the oxide

c^E = equilibrium solubility of the oxidant in the oxide

D_e = effective diffusion coefficient

h = gas phase mass transfer coefficient

k = rate constant of chemical surface reaction

n = unit outward normal vector

Note: c^E is related to the partial pressure of the oxidant in the gas via Henry's law.

D_e is dependent upon temperature and pressure.

k is a function of temperature.

2.2 Modelling Kinetics

Following the chemical reaction between the oxidising species and the silicon substrate, stresses are produced on the silicon/oxide interface by the non-uniform growth of the oxide. Since the silicon bulk is considerably more rigid than the oxide layer, a simplifying assumption is that of zero strain in the

silicon. This infers that the energy generated at the interface is completely expended on the displacement of the silicon dioxide and a conformable deformation of the nitride mask.

Figure 2 portrays a section of the silicon/oxide interface at some instant of time, t.

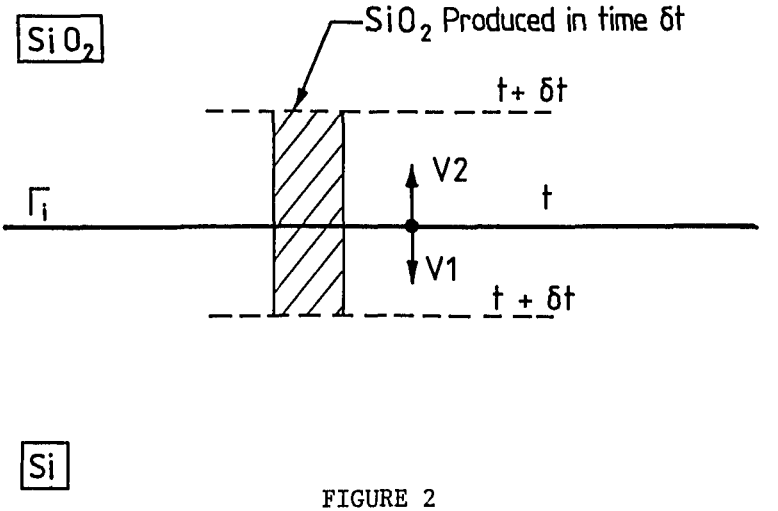

FIGURE 2

During a short period of time, δt, fresh oxide is produced in a quantity which is proportional to the flux of oxidant across the silicon/oxide interface.

From the law of conservation of mass, the absolute growth velocity of the silicon dioxide may be expressed in the following form:

$$V(t) = \frac{k.c(t)}{N1} \tag{5}$$

where N1 is the number of oxidising molecules per unit volume of oxide. The absolute velocity may then be resolved into two constituent parts, viz:

the silicon consuming velocity, which is defined as:

$$V1(t) = d\,\frac{k.c(t)}{N1} \tag{6}$$

and the oxide expanding velocity,

$$V2(t) = (d-1)\,\frac{k.c(t)}{N1} \tag{7}$$

where d is the density ratio of SiO_2:Si (=0.44), and the velocity vectors V1(t) and V2(t) are in the direction of the outward normal from the oxide at the interface.

2.3 Boundary Motion

The proposed hypothesis is that the growth of a field oxide on a silicon substrate may be considered to be incrementally linear elastic over a certain range of temperature, conservatively regarded as being below 960°C. The linear theory of elasticity for solids is based on the following two assumptions:

i) that the material is not stressed beyond the porportionality limit. For most engineering materials, it is assumed that the proportionality limit and the elastic limit are coincident. A corollary of this principle is that the displacement caused at any point in the material is linearly dependent on the magnitude of the applied loading.

ii) that the change in the domain orientation due to the induced displacements is negligible. If the deflections change the domain geometry in a significant way, the manner in which the potential energy is stored in the material changes and the load increases will not then cause a proportionate increase in displacement.

Great care should therefore be exercised in respect of the above maxims and their relevance to the current investigation, particularly with regard to the critical length of the time-steps.

The governing equation for the elastic displacement of the oxide and nitride layers may be written in terms of σ, the stress field components. Ignoring body forces, we have:

$$\frac{\partial \sigma_{ij}}{\partial x_j} = 0 \qquad i,j = 1,2 \tag{8}$$

We require a solution which satisfies the following boundary conditions:

$$u_j = V2_j.\delta t \qquad j\varepsilon\ \Gamma_1 \tag{9}$$

$$\left.\begin{aligned} u_1 &= 0 \\ \sigma_{2j}n_j &= 0 \end{aligned}\right\} \qquad j\varepsilon\ \Gamma_4 \tag{10}$$

$$\sigma_{ij}n_j = 0 \qquad j\varepsilon\ \Gamma_2 \cup \Gamma_3 \cup \Gamma_5 \qquad i=1,2 \tag{11}$$

where u_j represents the vector of prescribed displacements and n_j are the direction cosines of the outward normal with respect to the coordinate axes. Plane strain is assumed.

3. BOUNDARY ELEMENT FORMULATION

The numerical methods most widely in use today are 'domain' methods, such as Finite Elements or Finite Differences, which seek to resolve the governing differential equations in their derived forms. Since the accuracy of these methods is directly related, inter alia, to the fineness of the discretization mesh, it is inevitable that for most practical applications, large systems of simultaneous equations are generated during the solution procedure.

The Boundary Element Method adopts the approach of integrating the set of differential equations analytically before proceeding to a discretization scheme. This technique has the effect of reducing the governing equations to a set of independent equations involving only the variable values on the boundary of the domain. Consequently, for a homogeneous region, any necessary discretization plan simply involves subdivision of the surface of the body, and the solution is completely continuous inside the region.

Thus, the dimensionality of the problem is reduced by one, with consequent simplification of the data preparation and considerably lower matrix reduction requirements, which more than compensate for the fact that BEM system matrices are fully populated or, at best, block-banded, and generally non-symmetric.

Once the variable values have been computed on the boundary of the domain of interest, solution variables may then be calculated at any selected interior point, and high resolution information may be provided in zones of particular importance.

The Boundary Element Method can be applied to any situation where the governing differential equations are linear or are assumed to be incrementally linear. The very nature of the formulation makes it amenable to problems of moving boundaries, and its application to D'Arcy and Navier's equations is well established.

This work adopts the so-called 'direct' method of analysis [1], since it appears more versatile than other formulations and has the distinct added advantage of producing the physical variables as solution parameters. The numerical procedure is based upon a weighted residual technique, and the weighting functions are derived from the unit solution Green functions.

3.1 Species Diffusion

Consider the problem defined previously by equations (1) to (4). In this work, because we have assumed the diffusion

parameters to be dependent only upon the process data, equation (1) reduces to the following D'Arcy equation for isotropic materials:

$$D_e \left(\frac{\partial^2 c}{\partial x_i^2}\right) = 0 \qquad i=1,2 \tag{12}$$

Utilizing equation (12) and the boundary conditions supplied by (2), (3) and (4), the following weighted residual statement may be written:

$$\int_\Omega D_e\left(\frac{\partial^2 c}{\partial x_i^2}\right) c^* \, d\Omega = \int_{\Gamma_1} (c-\bar{c})q^* \, d\Gamma + \int_{\Gamma_2} (q-\bar{q})c^* \, d\Gamma \tag{13}$$

where $q = D_e \frac{\partial c}{\partial n}$

$$q^* = D_e \frac{\partial c^*}{\partial n}$$

If the left hand side of equation (13) is integrated twice by parts, we obtain the inverse formulation, viz:

$$\int_\Omega D_e \left(\frac{\partial^2 c^*}{\partial x_i^2}\right) c \, d\Omega = \int_{\Gamma_1} \bar{c}q^* \, d\Gamma + \int_{\Gamma_2} cq^* \, d\Gamma - \int_{\Gamma_1} qc^* \, d\Gamma - \int_{\Gamma_2} \bar{q}c^* \, d\Gamma \tag{14}$$

We now require to find a solution satisfying the second order D'Arcy equation $D_e\left(\frac{\partial^2 c^*}{\partial x_i^2}\right) = 0$.

If it is assumed that a concentrated change is acting at a point 'i', then we may write this governing equation as:

$$D_e \left(\frac{\partial^2 c^*}{\partial x_i^2}\right) + \delta_i = 0 \tag{15}$$

where δ_i is the Dirac delta function.

The solution, c^*, of equation (15) is known as the Fundamental Solution or Green's Function.
Then, by definition,

$$D_e\left(\frac{\partial^2 c^*}{\partial x_i^2}\right) \, d\Omega = - c_i \tag{16}$$

Equation (14) may be written more concisely as:

$$K_i c_i + \int_\Gamma cq^* \, d\Gamma = \int_\Gamma qc^* \, d\Gamma \tag{17}$$

where K_i takes a value between 0 and 1 depending on the location of the point 'i'.

The fundamental solution for a two dimensional isotropic medium is given as:

$$c^* = -\frac{1}{2\pi D_e} \ln r_o \tag{18}$$

$$q^* = -\frac{1}{2\pi D_e} \frac{\partial}{\partial n} (\ln r_o) \tag{19}$$

where $r_o = r/\sqrt{D_e}$, and r is the distance from the point of application of the unit charge to the point under consideration, the field point.

The boundary of the domain of interest may be divided into m elements, of which m_1 belongs to Γ_1 and m_2 belongs to Γ_2.

The discretized form of equation (17) is then

$$K_i c_i + \sum_{j=1}^{m} \int_{\Gamma_j} c q^* \, d\Gamma = \sum_{j=1}^{m} \int_{\Gamma_j} q c^* \, d\Gamma \tag{20}$$

This equation applies for each discrete point on the boundary, say node 'i', and the integral terms relate the ith node with the jth element.

Equation (20) may be rewritten as:

$$K_i c_i + \sum_{j=1}^{m} \hat{H}_{ij} c_j = \sum_{j=1}^{m} G_{ij} q_j \tag{21}$$

We may define the following relationship:

$$H_{ij} = \hat{H}_{ij} + K_i c_i \Delta_{ij} \tag{22}$$

where Δ_{ij} is the Kronecker delta.

Hence, equation (21) may be written in the general form:

$$\sum_{j=1}^{m} H_{ij} c_j = \sum_{j=1}^{m} G_{ij} q_j \tag{23}$$

The whole set of equations may then be expressed in matrix form as:

$$\underset{\approx}{H}\ \underset{\sim}{C} = \underset{\approx}{G}\ \underset{\sim}{Q} \tag{24}$$

From the applied boundary conditions, m_1 values of c are known, and m_2 values of q are also known, so we have a set of m equations with m unknowns. Equation (24) is then re-ordered to place all of the unknowns into a vector X, hence

$$\underset{\approx}{A}\ \underset{\sim}{X} = \underset{\sim}{F} \tag{25}$$

thereby all of the values of concentration and normal fluxes on the boundary of the domain may be established.

3.2 Elastic Displacement

Following the same approach used for the linear diffusion of the oxidising species, we may write a similar weighted residual statement which incorporates the governing equation (8) and the boundary conditions (9), (10) and (11).

$$\int_{\Omega} \left(\frac{\partial \sigma_{jk}}{\partial x_j}\right) u_k^* \, d\Omega = \int_{\Gamma_1} (\bar{u}_k - u_k) t_k^* \, d\Gamma + \int_{\Gamma_2} (t_k - \bar{t}_k) u_k^* \, d\Gamma \tag{26}$$

where u^* and t^* are the displacements and surface force intensities corresponding to the weighting field given below:

$$t_k^* = n_j \, \sigma_{jk}^* \qquad j,k = 1,2 \tag{27}$$

Assuming linear material behaviour, the strains at any point of the domain of interest may be written in terms of the strain field components, viz:

$$\varepsilon_{ij} = \frac{1}{2}\left(\frac{\partial u_i}{\partial x_j} + \frac{\partial u_j}{\partial x_i}\right) \qquad i,j = 1,2 \tag{28}$$

This relationship may be assumed to apply for both the approximating and the weighting fields.

Integrating the left-hand side of equation (26) twice, by parts, and utilizing the assumptions of equation (28), we have

$$\int_{\Omega} \left(\frac{\partial \sigma_{jk}^*}{\partial x_j}\right) u_k \, d\Omega = \int_{\Gamma_1} \bar{u}_k t_k^* \, d\Gamma + \int_{\Gamma_2} u_k t_k^* \, d\Gamma - \int_{\Gamma_1} t_k u_k^* \, d\Gamma - \int_{\Gamma_2} \bar{t}_k u_k^* \, d\Gamma \tag{29}$$

We now require the fundamental solution satisfying the equation $\frac{\partial \sigma_{jk}^*}{\partial x_j} = 0$. If it is assumed that a unit load is acting at a point 'i', in one of the x_ℓ directions, we may write this governing equation as

$$\frac{\partial \sigma_{jk}^*}{\partial x_j} - \delta_\ell^i = 0 \tag{30}$$

where δ_{ℓ}^{i} is the Dirac delta function and represents the unit load at 'i' in the 'ℓ' direction. This type of solution will produce the following equation for each direction 'ℓ'

$$K_i u_{\ell}^{i} + \int_{\Gamma_1} \bar{u}_k t_k^* \, d\Gamma + \int_{\Gamma_2} u_k t_k^* \, d\Gamma = \int_{\Gamma_1} t_k u_k^* \, d\Gamma + \int_{\Gamma_2} \bar{t}_k u^* \, d\Gamma \qquad (31)$$

Equation (31) may be written more concisely as:

$$K_i u_{\ell}^{i} + \int_{\Gamma} u_k t_k^* \, d\Gamma = \int_{\Gamma} t_k u_k^* \, d\Gamma \qquad (32)$$

where K_i takes a value between 0 and 1, depending on the location of the point 'i'.

The fundamental solution for a two-dimensional isotropic solid is given as:

$$u_{\ell k}^* = \frac{-1}{8\pi G(1-\nu)} \left[\frac{\partial r}{\partial x_{\ell}} \frac{\partial r}{\partial x_k} - (3-4\nu)\ell n \; r \right] \qquad (33)$$

$$t_{\ell k}^* = \frac{1}{4\pi(1-\nu)r} \left[\frac{\partial r}{\partial n} \{(1-2\nu)\Delta_{k\ell} + 2 \frac{\partial r}{\partial x_k} \frac{\partial r}{\partial x_{\ell}}\} - (1-2\nu) \{\frac{\partial r}{\partial x_{\ell}} n_k - \frac{\partial r}{\partial x_k} n_{\ell}\} \right] \qquad (34)$$

where $u_{\ell k}^*$ and $t_{\ell k}^*$ represent the displacements and surface force intensities in the 'k' direction due to an applied unit force in the direction 'ℓ', $\Delta_{\ell k}$ is the Kronecker delta, and r is the distance from the point of application of the unit load to the point under consideration, the field point.

In matrix form $\underset{\approx}{u}^*$ and $\underset{\approx}{t}^*$ are 2x2 matrices with elements $u_{\ell k}^*$ and $t_{\ell k}^*$.

The boundary displacements and tractions are expressed as vectors, viz:

$$\underset{\sim}{u} = \begin{bmatrix} u_1 \\ u_2 \end{bmatrix} \qquad \underset{\sim}{t} = \begin{bmatrix} t_1 \\ t_2 \end{bmatrix}$$

Equation (32) may also be expressed in matrix form as:

$$\underset{\approx}{K}_i \underset{\sim}{u}_i + \int_{\Gamma} \underset{\sim}{u} \, \underset{\approx}{t}^* \, d\Gamma = \int_{\Gamma} \underset{\sim}{t} \, \underset{\approx}{u}^* \, d\Gamma \qquad (35)$$

The boundary of the domain of interest may be divided into m elements, of which m_1 belong to Γ_1 and m_2 belong to Γ_2, $\Gamma_1 + \Gamma_2 = \Gamma$. The discretized form of equation (35) is then:

$$\underset{\sim}{K}_i \underset{\sim}{u}_i + \sum_{j=1}^{m} \int_{\Gamma_j} \underset{\sim}{u} \underset{\sim}{t}^* \, d\Gamma = \sum_{j=1}^{m} \int_{\Gamma_j} \underset{\sim}{t} \underset{\sim}{u}^* \, d\Gamma \qquad (36)$$

This equation applies for each discrete point on the boundary, say node 'i', and the integral terms relate the ith node with the jth element. The integral terms in equation (36) may be denoted by $\hat{\underset{\sim}{H}}_{ij} \underset{\sim}{u}_j$ and $\underset{\sim}{G}_{ij} \underset{\sim}{t}_j$, where $\hat{\underset{\sim}{H}}_{ij}$ and $\underset{\sim}{G}_{ij}$ are 2x2 matrices.

Then equation (36) may be re-written in the form

$$\underset{\sim}{K}_i \underset{\sim}{u}_i = \sum_{j=1}^{m} \hat{\underset{\sim}{H}}_{ij} \underset{\sim}{u}_j = \sum_{j=1}^{m} \underset{\sim}{G}_{ij} \underset{\sim}{t}_j \qquad (37)$$

We may define the following relationship:

$$\underset{\sim}{H}_{ij} = \hat{\underset{\sim}{H}}_{ij} + \underset{\sim}{K}_i \underset{\sim}{u}_i \underset{\sim}{\Delta}_{ij} \qquad (38)$$

where $\underset{\sim}{\Delta}_{ij}$ is the Kronecker delta matrix, $\underset{\sim}{K}_i$ is a coefficient matrix depending upon the boundary geometry.

Hence, equation (37) may be expressed in the general form:

$$\sum_{j=1}^{m} \underset{\sim}{H}_{ij} \underset{\sim}{u}_j = \sum_{j=1}^{m} \underset{\sim}{G}_{ij} \underset{\sim}{t}_j \qquad (39)$$

The whole set of equations can then be put into matrix form as:

$$\underset{\sim}{H} \, \underset{\sim}{U} = \underset{\sim}{G} \, \underset{\sim}{T} \qquad (40)$$

From the applied boundary conditions, $2m_1$ values of u are known and $2m_2$ values of t are also known, so we have a set of 2m equations with 2m unknowns.

Equation (40) may then be re-ordered to place all of the unknowns into a vector X, hence

$$\underset{\sim}{A} \, \underset{\sim}{X} = \underset{\sim}{F} \qquad (41)$$

thereby all of the values of displacement and surface force intensities on the boundary of the domain can be established.

4. ERROR ANALYSIS

The boundary integral equations (17) and (32) are themselves precise statements of the physical situation, and the principal errors which arise in the numerical computations are entirely related to the introduction of approximations in the domain geometry and the computational procedures. This section describes the three primary error-inducing mechanisms which contribute to inaccuracies in boundary element formulations, and proposes methods by which the errors may be controlled and prescribed accuracies achieved.

4.1 Discretization of the Space Domain

The domain geometry may be approximated as closely as the analyst deems necessary by the use of a parametric representation on the boundary. High solution accuracy and boundary definition may be achieved by using a mesh of linear elements, suitably refined in the vicinity of the bird's beak, or alternatively by the introduction of fewer elements with higher order shape functions.

From a practical standpoint, the extra accuracy obtained with the higher order elements has to be balanced against the inevitable increase in computational expense, and the most cost-effective discretization scheme adopted.

4.2 Discretization of the Time Domain

The standard approach to the numerical solution of a differential equation is to approximate the function curve by a sequence of line segments. The simplest and best-known of these techniques is a one-step explicit scheme, known as Euler's Method, whereby the value of the function at the end of the interval is calculated from the gradient of the function at the start of the interval. In the oxidation context, this approach involves the use of the interface fluxes at time t to predict the displacement of the oxide domain, and hence the new position at time $t+\delta t$.

Although this approach is conceptually very easy, it has a relatively high truncation error when compared with a Taylor series solution, and is often unstable in practice. These limitations are reflected in the size of the timesteps employed, which may need to be relatively small to achieve desired accuracies.

We now consider another of the broad class of Runge-Kutta Methods, a two-step explicit scheme, often referred to as the Improved Euler Method or Heun's Method, in which predictions are made on the basis of the average of the function gradients at the start and end of the timestep.

Let us re-write equation (6), describing silicon consuming velocity V1, in the following form:

$$\frac{du_i}{dt} = \frac{\rho_o}{\rho_s} \frac{kc(t)}{N1} n_i \qquad i=1,2 \qquad (42)$$

where u_i is the displacement of the interface into the silicon substrate in each of the coordinate directions, n_i is the unit outward normal vector from the oxide domain at the silicon/oxide interface, ρ_s is the density of silicon and ρ_o the density of silicon dioxide.

Equation (42) may be integrated numerically with respect to time to obtain an equation describing boundary displacement, viz:-

$$u_i\ (t+\delta t) = u_i(t) + \int_t^{t+\delta t} \frac{\rho_o}{\rho_s} \frac{kc(t)}{N1} n_i\ dt \qquad (43)$$

leading to:

$$u_i(t+\delta t) = u_i(t) + \frac{\delta t}{2}\left\{\frac{d\ k\ c}{N1} n_i\right\}\Big|_t + \frac{\delta t}{2}\left\{\frac{d\ k\ c}{N1} n_i\right\}\Big|_{t+\delta t} \qquad (44)$$

Similarly, the Dirichlet boundary condition for elastic displacement described by equation (9) may be written in the following form:

$$u_i(t+\delta t) = u_i(t) + \frac{\delta t}{2}\left\{\frac{(d-1)k\ c}{N1} n_i\right\}\Big|_t + \frac{\delta t}{2}\left\{\frac{(d-1)k\ c}{N1} n_i\right\}\Big|_{t+\delta t} \qquad (45)$$

The solving of equations (44) and (45) is an iterative procedure, since the evaluations of the functions at time t+δt must be made on the temporary domain determined by provisional displacements calculated at time t.

Although Heun's Method effectively doubles the time of computation, it produces results which are at least an order of magnitude more accurate than those obtained by the basic Euler Method. This enables longer time steps to be used and significantly reduces the overall computer simulation time.

4.3 Efficient Quadrature of the Matrix Coefficients

Figure 3(i) shows a pad oxide domain Ω_1 in the presence of a nitride mask, and Figure 3(ii) displays the same region of

interest at some intermediate or final stage of oxidation.

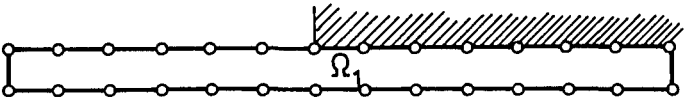

(i) Initial Domain

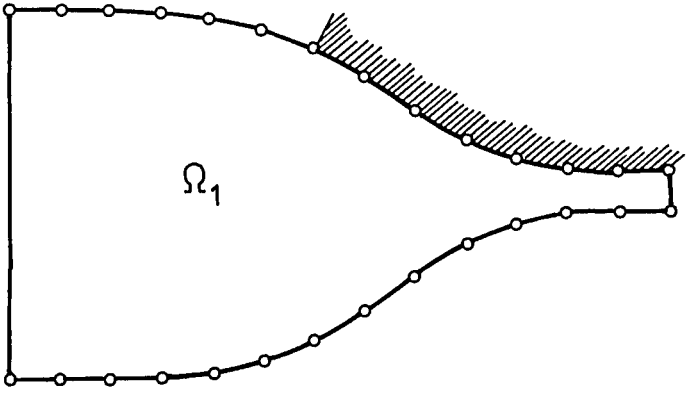

(ii) Secondary Domain

FIGURE 3

Now it appears that a major limitation of the finite element formulation of the oxidation process is the necessary regeneration of the discretization mesh at each timestep, which has previously proved costly in CPU time.

An immediate advantage of the Boundary Element Method in this situation is that any mesh refreshment is confined to the boundary of the domain, leading naturally to a more efficient solution procedure.

However, a perception of Figure 3(ii) will reveal that, for the linear problem at least, if the 'left and right hand' no-flow boundaries can be represented each by a single linear element, then the discretization of the domain boundary effectively reduces to a set of elements on the 'top and

bottom' boundaries of the dioxide layer. This ploy enables the modeller to allow the nodal points merely to adopt their displaced coordinate values at each subsequent timestep, thereby maintaining the initial number of nodes throughout, but with no appreciable loss in definition of the domain geometry.

This tactic introduces a relatively large element into the proceedings which leads to potentially disastrous consequences so far as the accurate integration of the matrix coefficients is concerned, and it is essential that preventative measures are taken to preserve the integrity of the quadrature. The following text outlines the precautions taken in this direction.

It may be observed that the fundamental solutions for both the D'Arcy equation governing steady state diffusion, and Navier's equation governing elastic displacement, are functions of $\ell n\ r$ and $1/r^2$, where r is the distance between the so-called source and observation points. It is well known that $\ell n\ r$ becomes weakly singular and $1/r^2$ becomes strongly singular as $r \to 0$. This situation pertains when the source points and integration regions are close together, and then the matrix coefficient integrand varies rapidly.

When quadrature is carried out by the Gauss-Legendre method, it is therefore crucial that the portion of the integration region nearest to the source point is allocated a large number of sampling points, so that desired levels of precision may be achieved. Conversely, when the source point is further away from parts of the observation region, the integrand is well-behaved, and far fewer Gauss points are required to maintain accuracy.

For the efficient implementation of the Boundary Element Method, it is therefore very important that the order of the chosen Gauss Rule is consistent with the prescribed accuracy of integration which, in turn, is dependent upon the relative value of r compared with the dimensions of the region of integration.

When the source point is very close to the observation region, or the region of integration is large, it may be that the maximum order of Gauss Rule contained within the program is too low to ensure that the desired accuracies are maintained. In this case, it becomes necessary to sub-divide the region of integration into a number of sub-regions, and each of these is then allocated its own coordinate axes, is integrated separately, and the results aggregated to give the overall value for the required matrix coefficient.

In this work, the diagonal entries of the G matrices are calculated analytically, and those of the H matrices by the application of rigid body motion. The off-diagonal matrix

coefficients are computed by Gaussian Quadrature, using 2, 4, 6 or 10 sampling points according to a pre-defined criterion.

The procedure devised for the numerical integration of the non-singular integrals is based on the work of Lachat and Wilson [3], and Liu Jun et al. [4], which minimises the computational effort by specifying an upper bound for the integration error. This requires that the order of the Gauss rule is selected on the basis of the ratio of the distance between the nearest point on the loaded element and the source point, to the length of the field element, and also on the strength of the approaching singularity.

When necessary, the field element is sub-divided unequally according to an inverse calculation of the optimum length of sub-element consistent with the previous criterion and incorporating ten integration points. If the final sub-element is shorter than the optimum length for efficiency, a lower number of sampling points is automatically selected.

5. SOLUTION FLOW CHART FOR HEUN'S METHOD

Step 1 : Select an initial pad oxide thickness and a suitable timestep.
Set time = 0

Step 2 : Generate meshes on the boundaries of Ω_1 and Ω_2.

Step 3 : Compute concentration values on the boundary of Ω_1 according to equations (1) to (4).

Step 4 : Store nodal coordinate values.

Step 5 : Calculate the absolute growing velocity and resolve into its component parts according to equations (5) to (7).

Step 6 : Store silicon consuming velocity values.

Step 7 : Compute displacement values on the boundaries of Ω_1 and Ω_2 according to equations (8) to (11).

Step 8 : Store displacement values on Γ_2 to Γ_5.

Step 9 : Deform Γ_1 according to displacements calculated from $V1(t)$ in step 5, and Γ_2 to Γ_5 according to displacements computed in step 7.

Step 10: Repeat steps 3, 5 and 7.

Step 11: Calculate the corrected nodal displacements for the current timestep by averaging the values stored in steps 6 and 8 with those obtained in step 10.

Step 12: Deform meshes on the boundaries of Ω_1 and Ω_2 accordingly.

Step 13: Repeat step 3.

Step 14: Update elapsed time.

Step 15: Return to step 4 unless simulation time is complete.

6. CONTROL PARAMETERS

The Deal and Grove model [2] for one-dimensional oxidation gives oxide thickness x_o as a function of time, t:

$$x_o = \frac{A}{2}\left[\left(1 + \frac{t+\tau}{A^2/4B}\right)^{\frac{1}{2}} - 1\right] \tag{46}$$

Two limiting forms of equation (46) have been identified:

$$\text{(i)}\ x_o \cong \frac{B}{A}(t+\tau) \tag{47}$$

when $t << A^2/4B$

$$\text{(ii)}\ x_o \cong (Bt)^{\frac{1}{2}} \tag{48}$$

when $t >> A^2/4B$, $t >> \tau$

The coefficient B is referred to as the parabolic rate constant, and B/A as the linear rate constant. The temperature dependence of both these constants shows a variation of the form:

$$C_o \exp(-E/RT) \tag{49}$$

where C_o is a pre-exponential constant and E is an activation energy.

The following relationships have been established for the thermal oxidation process:

$$D_e = D_o \exp\left(\frac{-q\ E_A}{RT}\right) \tag{50}$$

$$k = k_o \exp\left(\frac{-q\ E_K}{RT}\right) \tag{51}$$

$$A = 2\ D_e\ (1/k + 1/h) \tag{52}$$

$$B = 2\ D_e\ c^E/N1 \tag{53}$$

$$\tau = (x_i^2 + Ax_i)/B \qquad (54)$$

where x_i is the oxide thickness prior to any controlled oxidation and not necessarily the pad oxide thickness.

For the purposes of this paper, all simulations have been carried out on <111> surface orientated silicon, and the data values used are listed in Table 1 et seq., and Table 2.

7. RESULTS

The numerical model described in the foregoing text was used to simulate the problem of semi-recessed oxidation in a wet ambient at a process temperature of 920°C. The pad oxide thickness was assumed to be 25nm, with a nitride mask thickness of 100 nm.

The space discretization comprised 82 linear elements on the boundary of the oxide domain and 42 linear elements on the boundary of the nitride domain. The simulations were carried out for 200 minutes using 10 minute timesteps.

Table 3 gives a comparison of the computational 1-D errors incurred using Euler's Method and Heun's Method respectively and Figure 4 shows the final simulation geometry after 200 minutes.

ACKNOWLEDGEMENT

The authors wish to acknowledge the financial support for this work by the Science and Engineering Research Council as part of an Alvey project.

REFERENCES

1. C. A. BREBBIA
'The Boundary Element Method for Engineers', Pentech Press Ltd., Plymouth, 1978.

2. B. E. DEAL and A. S. GROVE
'General Relationship for the Thermal Oxidation of Silicon' Journal of Applied Physics, Vol.36, No.12, 1965.

3. J. C. LACHAT and J. O. WATSON
'Effective numerical treatment of boundary integral equations', Int. J. Num. Methods in Eng., Vol.10, 1976.

4. LUI JUN, G. BEER and J. L. MEEK
'Efficient evaluations of integrals of order $\frac{1}{r}$, $\frac{1}{r^2}$, $\frac{1}{r^3}$ using Gauss quadrature'. Engineering Analysis, Vol.2, No.3, 1985.

	O_2	H_2O
c^E (m^{-3})	5.20×10^{22}	3.00×10^{25}
N1 (m^{-3})	2.25×10^{28}	4.50×10^{28}
D_o (m^2s^{-1})	4.50×10^{-8}	3.54×10^{-9}
k_o (ms^{-1})	731.90	72.10
E_A (eV)	1.23	1.17
E_k (eV)	2.00	2.05

TABLE 1 - Diffusion Parameters

$q = 1.6 \times 10^{-19}$ Coulombs

$R = 1.38 \times 10^{-23}$ JK^{-1}

$h = 2.75$ ms^{-1}

	SiO_2	Si_3N_4
E (Nm^{-2})	6.60×10^{10}	3.89×10^{11}
ν	0.17	0.30

TABLE 2 - Elasticity Parameters

The above data values are assumed constant throughout the oxidation process.

Elapsed time (mins)	Deal & Grove 1-D Model (nm)	Euler's Method		Heun's Method	
		Absolute Error (nm)	Relative Error (%)	Absolute Error (nm)	Relative Error (%)
10	77.322	-4.858	-6.283	-0.036	-0.047
20	122.494	-7.220	-5.894	-0.046	-0.037
30	162.831	-8.572	-5.264	-0.049	-0.030
40	199.616	-9.415	-4.717	-0.051	-0.025
50	233.650	-9.971	-4.267	-0.052	-0.022
60	265.471	-10.348	-3.898	-0.051	-0.019
70	295.462	-10.610	-3.591	-0.047	-0.016
80	323.905	-10.793	-3.332	-0.039	-0.012
90	351.019	-10.920	-3.111	-0.025	-0.007
100	376.974	-11.006	-2.920	-0.001	0.000
110	401.907	-11.062	-2.752	0.032	0.008
120	425.930	-11.096	-2.605	0.077	0.018
130	449.136	-11.113	-2.474	0.135	0.030
140	471.603	-11.117	-2.357	0.206	0.044
150	493.397	-11.111	-2.252	0.292	0.059
160	514.576	-11.096	-2.156	0.394	0.076
170	535.189	-11.076	-2.070	0.511	0.095
180	555.279	-11.051	-1.990	0.644	0.116
190	574.883	-11.021	-1.917	0.793	0.138
200	594.036	-10.988	-1.850	0.959	0.161

TABLE 3 - Comparison of Time-stepping Methods

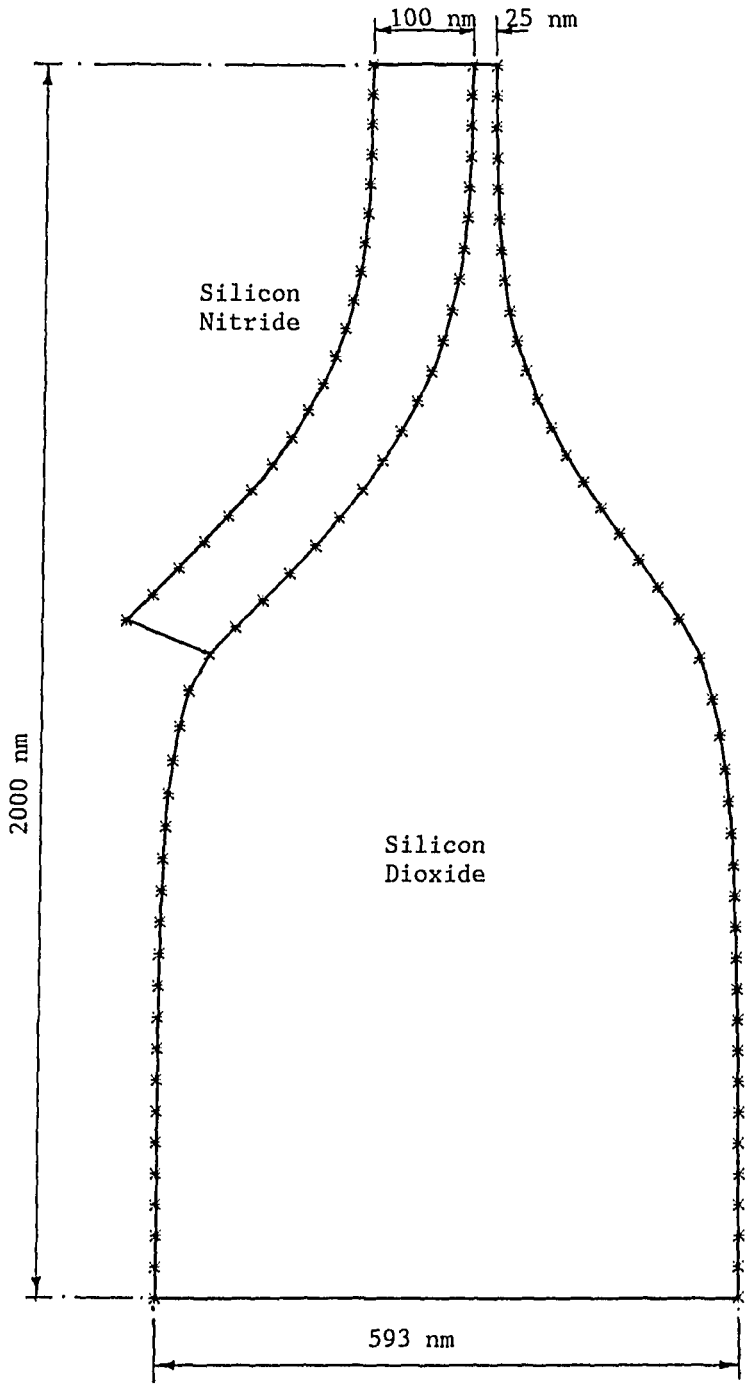

Figure 4 - Geometry after 200 minutes